Supervillin modulation of focal adhesions involving TRIP6/ZRP-1

Norio Takizawa,[1] Tara C. Smith,[1] Thomas Nebl,[1] Jessica L. Crowley,[1] Stephen J. Palmieri,[1] Lawrence M. Lifshitz,[2] Anka G. Ehrhardt,[1] Laura M. Hoffman,[3] Mary C. Beckerle,[3] and Elizabeth J. Luna[1]

[1]Department of Cell Biology, and [2]Department of Physiology, University of Massachusetts Medical School, Worcester, MA 01605
[3]Huntsman Cancer Institute, University of Utah, Salt Lake City, UT 84112

Cell–substrate contacts, called focal adhesions (FAs), are dynamic in rapidly moving cells. We show that supervillin (SV)—a peripheral membrane protein that binds myosin II and F-actin in such cells—negatively regulates stress fibers, FAs, and cell–substrate adhesion. The major FA regulatory sequence within SV (SV342-571) binds to the LIM domains of two proteins in the zyxin family, thyroid receptor–interacting protein 6 (TRIP6) and lipoma-preferred partner (LPP), but not to zyxin itself. SV and TRIP6 colocalize within large FAs, where TRIP6 may help recruit SV. RNAi-mediated decreases in either protein increase cell adhesion to fibronectin. TRIP6 partially rescues SV effects on stress fibers and FAs, apparently by mislocating SV away from FAs. Thus, SV interactions with TRIP6 at FAs promote loss of FA structure and function. SV and TRIP6 binding partners suggest several specific mechanisms through which the SV–TRIP6 interaction may regulate FA maturation and/or disassembly.

Introduction

Cell adhesion to the extracellular matrix plays an essential role during cell migration. Transmembrane integrins at focal adhesions (FAs) undergo cycles of matrix attachment, cytoskeletal recruitment, induction of contractile forces, and disassembly (Ridley et al., 2003). Nascent FAs form at or near anterior cell margins and mature into larger FAs under the middle and rear of the migrating cell. Some proteins, e.g., vinculin, are present for nearly the lifetime of a FA, whereas other proteins appear during maturation (Zaidel-Bar et al., 2004). Although both nascent and mature FAs are associated with stress fibers containing F-actin, α-actinin, and bipolar myosin II filaments (Zaidel-Bar et al., 2004), nascent FAs are responsible for most of the contractile forces (Beningo et al., 2001; Galbraith et al., 2002). Mature FAs retard the rate of cell translocation (Kaverina et al., 2002) and generate signals for cell survival and transcriptional activation (Alahari et al., 2002; Wang and Gilmore, 2003). FA disassembly/turnover is facilitated by Src family tyrosine kinases, adaptor proteins such as Crk, extracellular factor–regulated kinases (ERKs), selective proteolysis, and/or microtubules (Ridley et al., 2003; Carragher and Frame, 2004) and may be enhanced in fast-moving cells, such as immune cells and many tumor cells, especially invasive carcinomas (Kaverina et al., 2002; Carragher and Frame, 2004; Hogg et al., 2004).

Reorganization of FAs stimulated by mechanical cues involves zyxin and associated proteins (Yoshigi et al., 2005; Lele et al., 2006). The appearance of zyxin at FAs coincides with the loss of strong traction forces (Beningo et al., 2001), which is consistent with a role during maturation (Zaidel-Bar et al., 2004).

Other proteins related to zyxin found at mature FAs are lipoma-preferred partner (LPP; Petit et al., 2003) and thyroid receptor–interacting protein (TRIP6; Yi and Beckerle, 1998), which is also called zyxin-related protein 1 (ZRP-1) and Opa-interacting protein 1 (Zumbrunn and Trueb, 1996; Williams et al., 1998). Each zyxin family member contains an N-terminal domain that promotes local actin filament assembly and a C-terminal domain with three LIM domains, which are zinc finger motifs found in many cytoplasmic and nuclear proteins (Kadrmas and Beckerle, 2004).

The TRIP6 LIM domains bind to other proteins with LIM domains (Cuppen et al., 2000), to endoglin/CD105, which is a component of the TGF-β receptor complex (Sanz-Rodriguez

Correspondence to Elizabeth J. Luna: Luna@umassmed.edu

T. Nebl's present address is Department of Infection and Immunity, The Walter and Eliza Hall Institute of Medical Research, VIC 3050, Australia.

S.J. Palmieri's present address is Sensor Technologies, Shrewsbury, MA 01545.

Abbreviations used in this paper: ATCC, American Type Culture Collection; AV, archvillin; CAS, Crk-associated substrate; ERK, extracellular factor–regulated kinase; ds, double-stranded; FA, focal adhesion; LPA, lysophosphatidic acid; LPP, lipoma-preferred partner; PTP, protein tyrosine phosphatase; SmAV, smooth muscle AV; SV, supervillin; TRIP, thyroid receptor–interacting protein; ZRP-1, zyxin-related protein 1.

The online version of this article contains supplemental material.

The Journal of Cell Biology, Vol. 174, No. 3, July 31, 2006 447–458
http://www.jcb.org/cgi/doi/10.1083/jcb.200512051

Supplemental Material can be found at:
http://www.jcb.org/cgi/content/full/jcb.200512051/DC1

et al., 2004), to the protein tyrosine phosphatase (PTP) nonreceptor type 13 (PTPN13, PTP1E, FAP-1; Murthy et al., 1999; Cuppen et al., 2000), to Crk and the Crk-associated substrates (CAS) $p130^{Cas}$ and CASL/HEF1 (Yi et al., 2002), and to the membrane-bound, G protein–coupled lysophosphatidic acid 2 (LPA_2) receptor (Xu et al., 2004). The latter two interactions are potentiated by Src phosphorylation of Tyr-55 in TRIP6 (Lai et al., 2005), suggesting regulatory interactions between the TRIP6 N and C termini. The TRIP6 C terminus also binds to class 1 PDZ motifs (Cuppen et al., 2000; Harris and Lim, 2001), and the N terminus contains a nuclear export signal and transactivates gene expression (Wang and Gilmore, 2001; Kassel et al., 2004; Li et al., 2005).

TRIP6 has been implicated in the organization of actin filaments and in the control of cell migration with conflicting results. Knockdown of TRIP6 in human endothelial cells results in the disruption of cytoskeletal actin filaments (Sanz-Rodriguez et al., 2004). Overexpression of TRIP6 in mouse fibroblasts slows cell movements (Yi et al., 2002), whereas overexpression in SKOV3 ovarian carcinoma cells increases LPA-mediated cell migration and ERK activation (Xu et al., 2004; Lai et al., 2005). Nothing is known about the role of TRIP6 in cell–substrate adhesion or FA dynamics, leaving open questions about cell type–specific factors and regulation of different steps during cell migration.

In our exploration of membrane domains in highly motile cells, we have characterized a detergent-resistant plasma membrane fraction from neutrophils (Pestonjamasp et al., 1997; Nebl et al., 2002). This fraction contains F-actin, α-actinin, myosin II, cholesterol-organizing proteins, heterotrimeric G proteins, and the Src family kinase Lyn. The most tightly bound peripheral membrane protein, called supervillin (SV), is also relatively enriched in most carcinoma cell lines (Pestonjamasp et al., 1997; Pope et al., 1998).

SV binds tightly to F-actin and the S2 regulatory domain of myosin II, as well as to membranes (Pestonjamasp et al., 1997; Chen et al., 2003), and is implicated in both nuclear and membrane processes. Although SV contains functional NLS (Wulfkuhle et al., 1999) and can transactivate androgen receptor–mediated gene expression (Ting et al., 2002), ≥95% of total SV localizes with membranes in differentiated cells (Pestonjamasp et al., 1997; Oh et al., 2003). As the only membrane protein known to bind both myosin II and F-actin, SV may organize actin and myosin II filaments at the membrane and/or mediate actin-independent binding of myosin II to membranes (Nebl et al., 2002; Chen et al., 2003). SV sequences can induce F-actin cross-linking and bundling, myosin II mislocalization, and disruption of vinculin localization at ventral cell surfaces (Wulfkuhle et al., 1999; Chen et al., 2003). Alternatively spliced forms of SV, which are found in striated and smooth muscle (archvillin [AV] and smooth muscle AV [SmAV], respectively), are implicated in costamere organization, ERK signaling, contractility, and myogenic differentiation (Oh et al., 2003; Gangopadhyay et al., 2004).

We now show that SV promotes a process leading to the loss of cell–substrate adhesion and large FA. We have also identified the region of SV responsible for this activity as aa 342–571 and characterized relevant SV342-571 binding partners. SV-mediated down-regulation of FAs involves binding to TRIP6 and, possibly, also to LPP. SV and TRIP6 negatively regulate large FAs, either by blocking maturation or by facilitating disassembly. This interaction may regulate cell–substrate adhesion through the recruitment of actin and/or myosin II to TRIP6-associated signaling networks and could play a role in FA signaling to the nucleus.

Results

SV negatively regulates FA structure and function

EGFP-SV at low levels overlaps with vinculin at or near FAs on the basal surfaces of CV1 (Wulfkuhle et al., 1999) and COS7 (Fig. S1, available at http://www.jcb.org/cgi/content/full/jcb.200512051/DC1) cells. This overlap is more pronounced at large, mature FAs in the center and posterior of the cell than at newly formed FAs at the cell periphery (Fig. S1, arrow). SV also localizes along associated stress fibers; this signal increases disproportionately with increasing amounts of EGFP-SV (Wulfkuhle et al., 1999).

SV targeting to large FAs apparently reduces the number of these structures (Fig. 1). Large vinculin-labeled FAs are abundant in COS7 cells that overexpress EGFP (Fig. 1 A, a and b), but most large vinculin spots are lost in cells that overexpress EGFP-SV (Fig. 1 A, c and d). We find an ∼1:1 ratio of EGFP-SV to endogenous SV in lysates from preparations with ∼20% transfected cells (Fig. 1 B), indicating that the average level of EGFP-SV in the transfected cells is approximately five times greater than endogenous SV, for a total of approximately six times more SV than in untransfected cells. We normalized the amount of fluorescence in cells transfected with EGFP alone or EGFP-SV so that cells with approximately sixfold overexpression of SV exhibit ∼50% of maximal fluorescence intensity (Fig. 1 C). The number of large FAs (≥10 μm^2) in cells expressing EGFP-SV with ∼30–90% of maximal fluorescence are less than half those observed in cells expressing equivalent amounts of EGFP alone or in untransfected cells (Fig. 1, C and D). Thus, even an approximately threefold increase in SV levels down-regulates the number of large FAs.

Cell–substrate adhesion also correlates inversely with SV levels (Fig. 1, E and F). After preparative FACS, COS7 cells expressing EGFP-SV contain ∼6.3-fold more SV than cells expressing EGFP (Fig. 1 E, top) and are significantly less adherent to fibronectin-coated coverslips (Fig. 1 E, bottom). Conversely, cells with ∼10% of endogenous levels of SV adhere more tightly to fibronectin (Fig. 1 F, bottom). Collectively, these results show an inverse correlation between SV levels and FA function, although any increases in the number and/or size of mature FAs after SV knockdown lack statistical significance (unpublished data).

Identification of FA regulatory sequences

To identify SV sequences responsible for loss of FA integrity, we quantified the number of total and large FAs in COS7 cells expressing different EGFP-tagged SV constructs (Fig. 2).

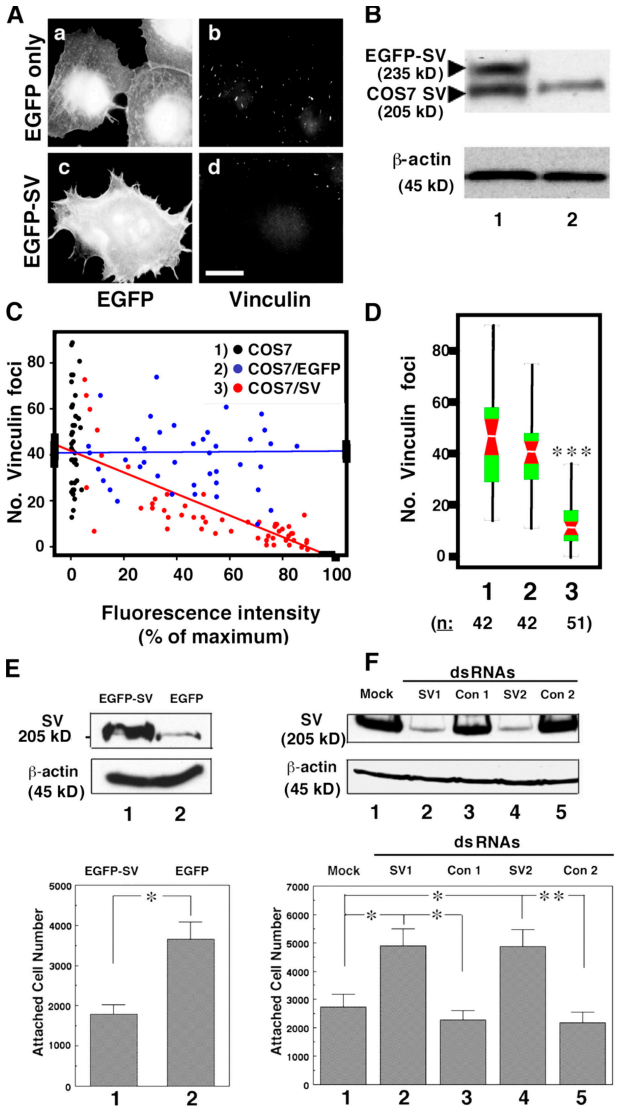

Figure 1. **Inverse correlation between SV levels and FA structure and function.** (A) Increasing levels of EGFP-SV (c and d), but not EGFP alone (a and b), decrease the number of FAs that stain brightly with anti-vinculin antibody (b and d). Bar, 10 μm. (B) Immunoblots of lysates from COS7 cells overexpressing EGFP-SV (lane 1) or EGFP (lane 2) stained with anti-SV antibody and for β-actin, as a loading control. (C) Scatter plot of vinculin-stained foci per cell versus relative intensity level of EGFP-SV (red) or EGFP alone (blue). Cells expressing <5% of maximal fluorescence were assumed to be untransfected (black). (D) Box plot of the data in C, showing medians (white lines), 95% confidence intervals (red) between the first and third quartiles (green), and minimal and maximal points (brackets) for untransfected (1), EGFP-expressing (2), and EGFP-SV–expressing (3) COS-7 cells. Number of cells (*n*), as shown. Differences between cells expressing EGFP-SV versus EGFP alone ($P = 0.0038$) or untransfected cells ($P \leq 0.001$) are statistically significant (***). (E) Immunoblot of SV levels in cells overexpressing EGFP-SV (lane 1) or EGFP (lane 2) and histogram of fibronectin-adhered cells after centrifugation (bottom). Mean ± the SEM. $n = 3$. *, $P < 0.05$. (F) Immunoblot of endogenous SV and (bottom) histogram of adherent cells showing that RNAi-mediated decreases in SV levels correlate with increased cell adhesion to fibronectin. Reagent alone (lane 1, Mock), dsRNAs 2,472 or 668 that target SV (lanes 2 and 4, SV1 and SV2), or control 2,472 Rev or 668con dsRNAs (lanes 3 and 5, Con 1 and Con 2). Endogenous SV (205 kD) was detected with anti-H340 antibody; β-actin was the loading control. Mean ± the SEM. $n = 4$. *, $P < 0.05$; **, $P < 0.01$.

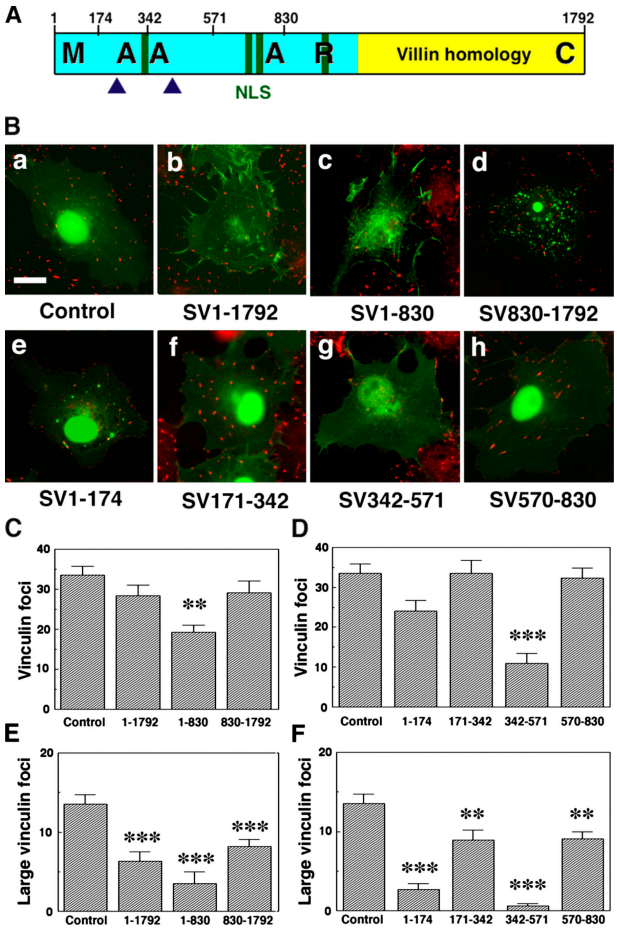

Figure 2. **Disruption of FA by SV sequences, especially SV1-174 and SV342-571.** (A) SV structure showing construct boundaries relative to binding sites for myosin II heavy chain (M), F-actin (A), androgen receptor (R), and calponin (C) and muscle-specific exons (arrowheads), nuclear localization sequences (NLS), and the villin/gelsolin homology region (villin homology). (B) Fluorescence micrographs showing vinculin (red) and EGFP-tagged chimeric proteins containing the designated SV amino acids (green). Bar, 20 μm. (C–F) Quantification of total (C and D) and large (E and F) vinculin-stained foci in COS7 cells expressing moderate levels of each EGFP chimera. Mean ± the SEM from 18–25 cells per construct. **, $P < 0.01$; ***, $P < 0.001$.

Full-length SV (Fig. 2 A, SV1-1792) reduces the number of large vinculin foci (Fig. 1 A–D and Fig. 2 E), but has relatively little effect on the number of the more abundant, smaller foci near cell peripheries (Fig. 2 B, b). The result is the absence of a statistically significant effect on the number of total FAs per cell (Fig. 2 C). The SV N terminus (SV1-830) decreases the number of both total and large FAs, whereas the SV C terminus (SV830-1792) exhibits effects similar to those of full-length SV (Fig. 2, B, C, and E). Thus, a sequence with major impact on FA stability resides within the SV N terminus.

Further dissection of N-terminal SV sequences identifies SV1-174 and SV342-571 as FA disruption sequences (Fig. 2, B, D, and F). Both of these sequences significantly reduce the number of large FAs (Fig. 2 F), but only SV342-571 significantly reduces the total number of vinculin foci per cell (Fig. 2 D).

COS-7 cells transfected with SV or SV N-terminal sequences also exhibit decreased numbers of large F-actin

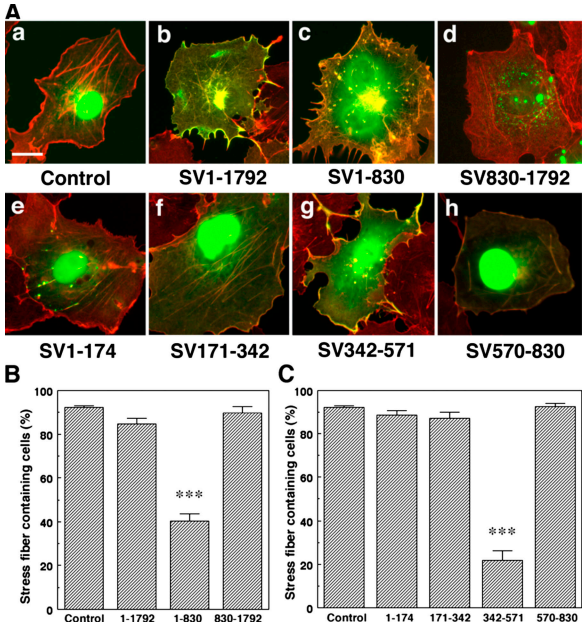

Figure 3. **Disruption of stress fibers by SV and fragments, especially SV342-571.** (A) Fluorescence micrographs showing phalloidin-stained F-actin (red) and EGFP-tagged chimeric proteins (green). Bar, 20 μm. (B and C) Percentages of transfected COS-7 cells expressing moderate levels of each EGFP chimera, and even one basal F-actin bundle. Mean ± the SEM. $n = 3$, 100 cells/experiment. ***, $P < 0.001$.

bundles (Fig. 3). Although full-length SV with its three F-actin–binding sites (Chen et al., 2003) increases the number of thin actin structures (Wulfkuhle et al., 1999), SV overexpression greatly decreases the number and size of large, straight actin bundles (Fig. 3 A, compare b with a). However, most SV-expressing cells still contain at least one large basal F-actin bundle (Fig. 3 B). Because most of these bundles exhibit periodic staining for α-actinin (Wulfkuhle et al., 1999) and myosin II (unpublished data), we refer to them here as "stress fibers," although they are smaller and less well organized than are stress fibers in fibroblasts.

Consistent with their effects on FA structure (Fig. 2), SV1-830 and SV342-571 significantly decrease the number of COS7 cells containing at least one stress fiber, as compared with cells expressing EGFP alone or other EGFP-SV fragments (Fig. 3, A–C). SV1-830 and SV342-571 also decrease the number and thickness of stress fibers in CV1 cells (unpublished data). Thus, SV342-571 contains a site that is primarily responsible for the morphological effects of SV and SV1-830 on FAs and stress fiber organization and function.

In support of this conclusion, SV342-571 reduces the contractility of CV1 cells (Fig. 4 and Table I). Significant percentages of cells expressing EGFP only or other EGFP-SV N-terminal sequences deform flexible silicon substrates, forming "wrinkles" (Fig. 4 and Table I). In contrast, wrinkles are absent from the areas around most CV1 cells expressing SV342-571 (Table I), even cells near untransfected cells that are actively wrinkling the substrate, thus, demonstrating its local deformability (Fig. 4 C, arrow vs. arrowhead). Thus, SV342-571 contains sequences capable of reducing FA structure and function.

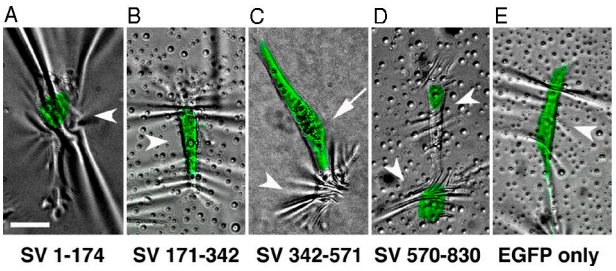

Figure 4. **SV342-571 reduces contractility of CV1 cells attached to gelatin-coated flexible silicon substrates.** Cells transfected with EGFP-SV1-174 (A), EGFP-SV171-342 (B), EGFP-SV342-571 (C), EGFP-SV570-830 (D), or EGFP alone (E) were scored for the presence of wrinkles (arrowheads; Table I). In contrast to transfected (A, B, D, and E) and untransfected (C, arrowhead) cells, CV1 cells expressing EGFP-SV342-571 (C, arrow) were largely unable to generate wrinkles. Micrographs show merges of differential interference contrast (gray scale) and EGFP (green) images. Bar, 20 μm.

Identification of SV342-571 binding partners

We hypothesized that a previously unknown interaction mediated the effects of SV342-571 on FAs. The only known binding partner for SV342-571 is F-actin (Fig. 2 A), but F-actin also binds to SV171-342 and SV570-830 (Chen et al., 2003), neither of which affects FA structure and function to the same extent (Figs. 2–4 and Table I). To identify candidate interactors with SV342-571, we undertook an undirected yeast two-hybrid screen. Because SV343-570, SV171-570, and SV343-830 all self-activated reporter gene expression (unpublished data), our bait plasmid encoded SV171-830. 11 prey proteins were identified and confirmed by directed yeast two-hybrid assays (Table II). These proteins were further screened using baits encoding either SV171-343 or SV570-830. Only the longer plasmid (SV171-830) containing SV343-570 sequences interacted strongly with the prey proteins.

Two interactors, TRIP6/ZRP-1 and Tctex-1/DYNLT1, account for a majority of the clones identified in these screens (Fig. 5). Ten independent clones encode all three C-terminal LIM domains of TRIP6. Another clone encodes the first two LIM domains of LPP, suggesting that two or more LIM domains are required for binding. Six independent clones encode full-length Tctex-1, which is a dynein light chain (DYNLT1).

We confirmed binding interactions with TRIP6 and Tctex-1 using pull-down assays with GST fusion proteins containing SV343-571 (Fig. 6). V5-tagged TRIP6 LIM domains (Fig. 6 A) and V5-tagged full-length Tctex-1 (Fig. 6 B) copellet

Table I. **Quantification of cell deformability**

EGFP construct	Wrinkled cell	Total cells	%	No. expts
SV1-174	15	28	54%	5
SV171-342	10	28	36%	4
SV342-571	2	31	6%	5
SV570-830	18	61	30%	4
EGFP only	20	29	69%	4

Pooled number of wrinkled cells, total cells, and percentages of wrinkled cells from 4–5 experiments with sparsely spread CV1 cells expressing the designated EGFP chimeric proteins. No. expts, number of experiments.

Table II. **Potential binding partners for SV342-571**

Interactor	Number of clones	Directed yeast two-hybrid assay results		
	(d1; d2; Ind)	SV171-830	SV171-343	SV571-830
TRIP6 (NM_003302)	17; 7; 10	++	–	–
Tctex-1 (NM_006519)	7; 9; 6	++	–	–
CXXCF1 (NM_014593)	2; 0; 1	++	–	+
GOLGA2 (NM_004486)	1; 0; 1	++	–	+
AMOTL2 (NM_016201)	1; 0; 1	++	–	–
LPP (NM_005578)	0; 1; 1	++	–	–
CTBP2 (NM_022802)	0; 1; 1	++	–	–
MAD1 (NM_003550)	0; 1; 1	++	–	+
AD023 (NM_020679)	0; 1; 1	++	–	–
GRP78 (NM_005347)	0; 1; 1	++	–	+
KIF4A (NM_012310)	0; 1; 1	++	–	+

Positive interactors for SV171-830 were identified in an untargeted yeast two-hybrid assay and screened for interactions with SV171-343 and SV571-830 in directed assays for leucine autotrophy and β-galactosidase. Names, nucleic acid accession numbers, the number of clones containing each interactor identified on day 1 (d1) or day 2 (d2), and the number of independent clones (Ind) are shown. ++, passed both requirements for positive interaction; +: passed β-galactosidase test only. In addition to TRIP6, LPP, and Tctex-1 (Fig. 5), potential interactors include the following: CXXC finger 1 (CXXCF1); Golgi autoantigen, golgin subfamily a, 2 (GOLGA2, GM130); angiomotin-like 2 (AMOTL2); C-terminal binding protein 2 (CTBP2); mitotic arrest deficient-like 1 (MAD1); glucose-regulated protein 78 kD (GRP78); and kinesin family member 4 (KIF4A).

with glutathione–Sepharose beads containing GST-tagged SV171-830, SV343-571, SV171-571, and SV343-830 (Fig. 6, A and B, lanes 2, 5, 7, and 8). Neither V5-tagged protein cosediments with beads containing GST only or SV171-342 (Fig. 6, A and B, lanes 3 and 4). A low-affinity interaction with SV570-830 is observed for Tctex-1 (Fig. 6 B, lane 6). No proteins reactive with the anti-V5 antibody are detectable in control yeast extracts (Fig. 6, A and B, lane 9), confirming the binding specificities of TRIP6 and Tctex-1 for SV342-571.

Binding of SV342-571 to TRIP6 or Tctex-1 is also observed in doubly transfected COS7 cells. Myc-tagged TRIP6 LIM domains and Tctex-1 cosediment with GST-tagged EGFP-SV342-571, but not with EGFP-GST alone (Fig. 6 C, lane 3 vs. 4). Notably, neither Myc-tagged LIM domains from zyxin nor Flag-tagged, full-length TRIP6 cosediments with EGFP-SV342-571-GST. Coimmunoprecipitation of full-length proteins was precluded by the inextractability of full-length SV (Pestonjamasp et al., 1997; Nebl et al., 2002).

The TRIP6 LIM domains and Tctex-1 bind directly to overlapping sequences within SV343-571 (Fig. 6, D–F). Purified, bacterially expressed hexahistidine (6×His)-tagged TRIP6 LIM domains (Fig. 6 D) and 6×His-Tctex-1 (Fig. 6 E) cosediment with glutathione–Sepharose beads containing prebound, purified GST-SV343-571 (Fig. 6, D and E, lane 2), but not with beads bound to GST alone (Fig. 6, D and E, lane 4). Increasing amounts of 6×His-tagged Tctex-1 compete with 6×His-tagged TRIP6 LIM domains for binding to a fixed, limiting amount of GST-SV343-571 (Fig. 6 F).

Point mutagenesis provides further support for competition between TRIP6 and Tctex-1 for binding to SV343-571. Conversion of the highly conserved SV residues Arg-426 and Tyr-427 to alanines (RY/AA) coordinately reduces binding of GST-SV343-571-RY/AA to both TRIP6 and Tctex-1 by ∼70% (Fig. 6 G). Similarly, mutagenesis of these residues in EGFP-SV343-571 reduces this protein's effects on stress fiber and FA structure (Fig. S2, available at http://www.jcb.org/cgi/content/full/jcb.200512051/DC1), demonstrating the functional importance of the TRIP6/Tctex-1–binding site within SV342-571.

Physiological relevance of the SV–TRIP6 interaction

To determine whether the SV interaction with TRIP6 and/or with Tctex-1 is involved in SV-mediated changes in FA structure and function, we colocalized these proteins in A7r5 (Fig. 7) and COS7 (Fig. 8) cells. Endogenous levels of the relatively abundant SmAV (Gangopadhyay et al., 2004) partially colocalize with endogenous vinculin (Fig. 7, b–d) and TRIP6 (Fig. 7, j–l) in A7r5 cells on fibronectin (Fig. 7, a, e, and i). The SmAV signal is a subset of that for vinculin and TRIP6 in FAs, but stops short of the labeling for these two proteins at cell edges. This result is consistent with a r ole for the SV– TRIP6 interaction in regulating adhesion, but is uninformative about Tctex-1 because we could not detect Tctex-1 in A7r5 cells (unpublished data).

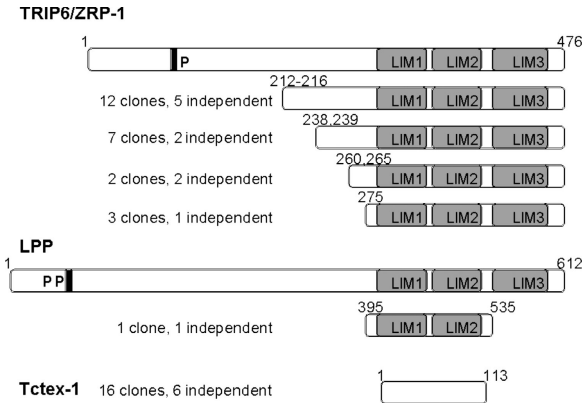

Figure 5. **TRIP6/ZRP-1 and Tctex-1/DYNLT1 are the prey proteins obtained most frequently in yeast two-hybrid screens with SV171-830 as bait.** Amino acid numbers of encoded prey proteins are shown, as are the locations of proline-rich (P) and nuclear export sequences (NES; black bars). Similarly sized independent clones are shown together with their N-terminal amino acids, e.g., five clones initiating at TRIP6 aa 212–216.

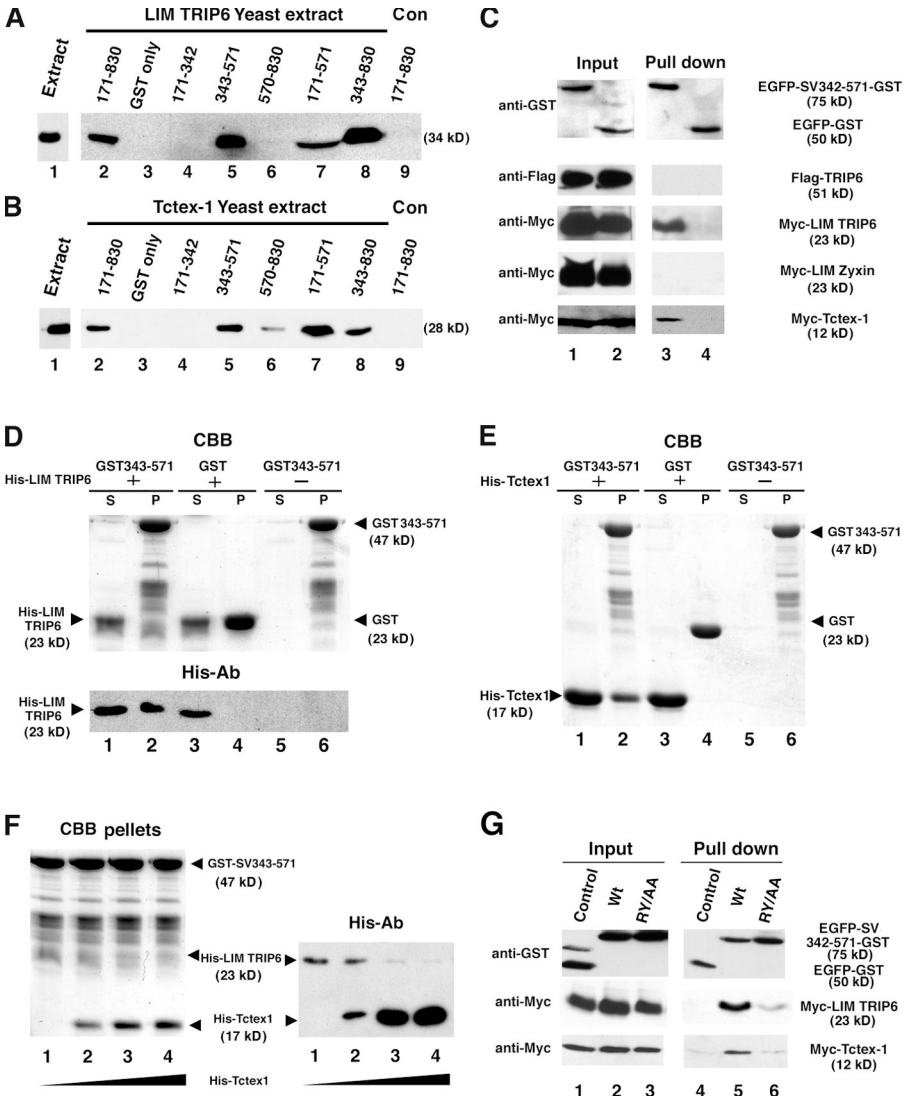

Figure 6. **SV343-571 binds to both TRIP6 and Tctex-1 in GST pull-down assays.** Immunoblots with anti-V5 antibody of extracts (A and B, lane 1) from yeast expressing V5-tagged TRIP6 LIM domains (A) or V5-tagged full-length Tctex-1 (B). Specifically bound proteins were eluted with glutathione from glutathione–Sepharose columns with prebound GST-tagged SV proteins (~1.0 nmol), as shown. V5-immunoreactive proteins were absent from control (Con) extracts (A and B, lane 9). (C) Immunoblots with anti-tag antibodies, as shown on the left, of COS-7 cell lysates (lanes 1 and 2) or lysate proteins eluted from glutathione–Sepharose (lanes 3 and 4). The COS-7 cells coexpressed either EGFP-SV342-571-GST (lanes 1 and 3, top) or EGFP-GST (lanes 2 and 4, top) and the tagged constructs indicated on the right. Although Flag-tagged full-length TRIP6 (second row) and Myc-tagged zyxin LIM domains (fourth row) bound neither GST protein, the Myc-tagged LIM domains of TRIP6 (third row) and Myc-tagged Tctex-1 (fifth row) each cosedimented with EGFP-SV342-571-GST, but not with EGFP-GST. Direct binding in vitro of 6×His-tagged TRIP6 LIM domains (D) and Tctex-1 (E) to purified GST-SV343-571 (D and E, lane 2). Supernatants (S; lanes 1, 3, and 5) and pellets (P; lanes 2, 4, and 6) from incubations with GST-SV343-571 and 6×His-proteins (lanes 1 and 2); GST alone and 6×His-proteins (lanes 3 and 4); or GST-SV343-571 alone (lanes 5 and 6). (F) Competition assay showing that increasing amounts of 6×His-Tctex-1 decreased binding of 6×His-TRIP6 LIM domains to GST-SV343-571. Bound proteins were detected with Coomassie blue (CBB) or immunoblotting with anti-6×His antibodies (His-Ab). (G) Binding of TRIP6 and Tctex-1 to EGFP-SV342-571-GST are comparably reduced by alanine replacement of SV R-426/Y-427. The COS-7 cells coexpressed either EGFP-GST (lanes 1 and 4, top), wild type (Wt) EGFP-SV342-571-GST (lanes 2 and 5, top), or the R426A/Y427A point mutant (RY/AA) in EGFP-SV342-571-GST (lanes 3 and 6, top). Affinity is reduced, both for Myc-tagged TRIP6 LIM domains (middle) and for Myc-tagged Tctex-1 (bottom).

In doubly transfected COS7 cells, Flag-TRIP6, but not Myc–Tctex-1, partially colocalizes with EGFP-SV and vinculin (Fig. 8). Although COS7 cells contain endogenous TRIP6 and Tctex-1 (Fig. S3, available at http://www.jcb.org/cgi/content/full/jcb.200512051/DC1), the epitope-tagged versions of these proteins are required for immunofluorescence. Full-length EGFP-SV and Flag-TRIP6 colocalize in membrane surface extensions that lack strong vinculin staining and along F-actin bundles, as well as with vinculin at FAs (Fig. 8, A and B, a–d and a'–d'). In contrast, little or no colocalization is seen between TRIP6 and the primarily nuclear EGFP (Fig. 8 C, e–h) or between Tctex-1 and either EGFP-SV or vinculin (Fig. 8 D, i–l), suggesting that TRIP6, rather than Tctex-1, mediates SV effects at FAs.

In fact, TRIP6 may help recruit SV to FAs. Although SV is not required for the FA localization of TRIP6 (Fig. S4, available at http://www.jcb.org/cgi/content/full/jcb.200512051/DC1), full-length EGFP-SV lacking the TRIP6-binding site is largely absent from FAs (Fig. 9, SVΔ343-561). Unlike EGFP-SV (Fig. 9, arrowheads, and Fig. S1), EGFP-SVΔ343-561 is associated with branched and curved actin filaments that appear to associate with vinculin foci at only one end (Fig. 9 B, arrows). Blind scoring of the percentage overlaps of EGFP signals with vinculin at large FAs shows overlap at 49.7 ± 8.8% of the FAs in cells expressing EGFP- SVΔ343-561, compared with 74.2 ± 6.1% in cells expressing EGFP-SV (mean ± SEM; $n = 220$ and 238 FAs from 15 cells each; $P < 0.03$). This decreased overlap with vinculin is probably an underestimate of TRIP6's effect on SV recruitment to FAs because the SV localization along filaments favors false positives.

TRIP6 also modulates adhesion of human A549 lung carcinoma cells to fibronectin (Fig. 10, A and B). RNAi-mediated knockdowns of TRIP6 (hTR1, hTR2), but not Tctex-1 (hTx), significantly increase adhesion (Fig. 10, A and B). This effect is comparable to that observed upon SV knockdown (hSV) and is consistent with the reported inverse correlation between TRIP6 levels and the number of large FAs (Guryanova et al., 2005).

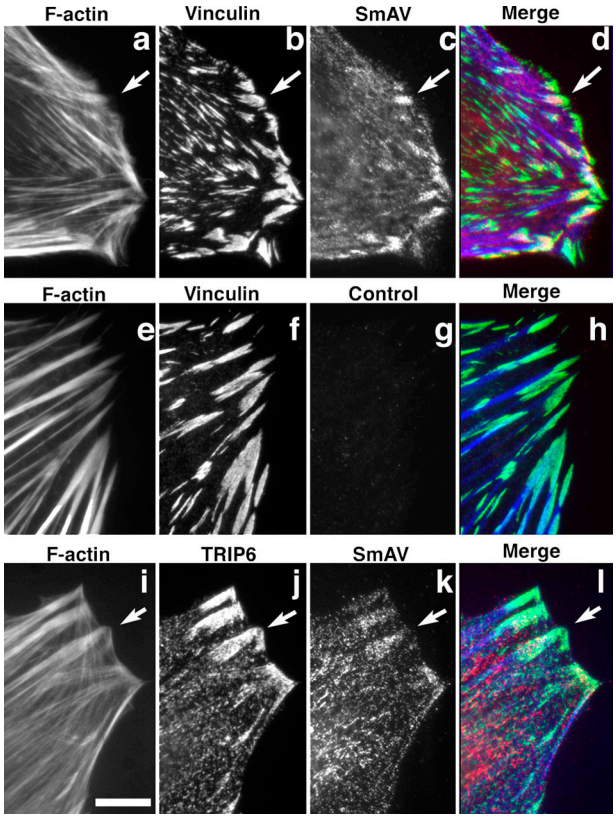

Figure 7. **Partial colocalization of endogenous TRIP6 and smooth muscle SV.** Immunofluorescence micrographs of fibronectin-plated, serum-starved A7r5 cells stained for F-actin (a, e, and i; blue in d, h, and l), vinculin (b and f; green in d and h), TRIP6 (j; green in l), and SmAV (c and k; red in d and l) show partial colocalization of SV and TRIP6 at FAs near, but not at, the cell periphery (arrows). No signal in the red channel was observed in the absence of anti-SV antibody (g). Bar, 10 μm.

TRIP6 sequences also partially reverse losses of stress fibers and large FAs induced by SV sequences capable of binding to these proteins (Fig. 10, C and D). Exogenously co-expressed TRIP6 LIM domains, but not zyxin LIM domains or Tctex-1, reduce the effects of SV domains, EGFP-SV1-830 and EGFP-SV342-571, on stress fibers in COS7 cells (Fig. 10 C). Full-length TRIP6 partially rescues the effects of full-length EGFP-SV (Fig. 10 D) and EGFP-SV1-830, although not that of SV342-571 (Fig. 10 C). The basis for the TRIP6-mediated rescue may be mislocalization of TRIP6–SV complexes because cells with high expression levels of both TRIP6 and EGFP-SV (Fig. 10 E) exhibit increased colocalization of TRIP6 and SV in protrusions lacking vinculin (Fig. 10 E, a–d, arrows, vs. Fig. 8 A). Rescued FAs contain TRIP6, but are largely devoid of EGFP-SV (Fig. 10 E, arrowheads). As expected, TRIP6 has no effect on the phenotype of point (SV-RY/AA) and deletion (SVΔ343-561) mutants of full-length SV that have reduced or no binding to TRIP6, respectively (Fig. 10, D and E [e–h]). Consistent with the observations that multiple SV sequences affect FA structure (Fig. 2, E and F), full-length SV mutants deficient in binding to TRIP6 induce a loss of large FAs in both the presence and absence of TRIP6 (Fig. 10 D). This result emphasizes the importance of additional SV-binding partners.

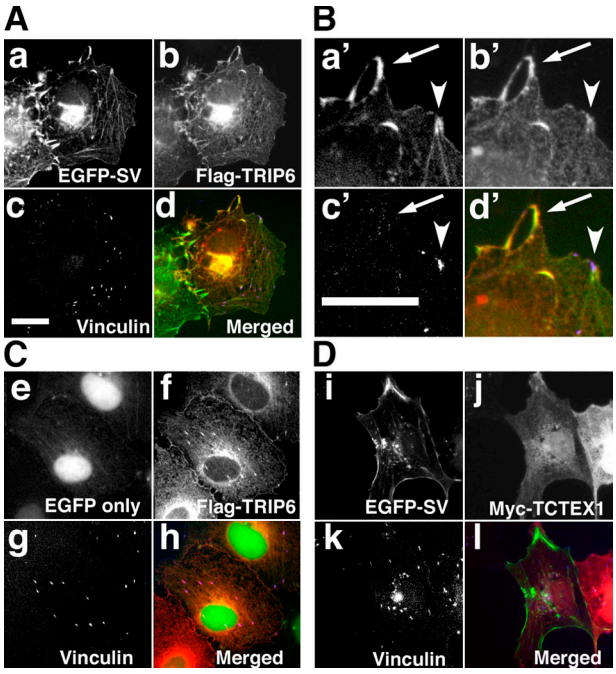

Figure 8. **Epitope-tagged TRIP6, but not Tctex-1, colocalizes with SV at FAs.** (A, B, and D) Micrographs of full-length EGFP-SV (a and i; green in d and l) or (C) EGFP alone (e; green in h) with Flag-TRIP6 (b and f; red in d and h) or Myc-Tctex-1 (j; red in l) in COS-7 cells counterstained with anti-vinculin (c, g, and k; blue in d, h, and l) and anti-Flag or anti-Myc antibodies. Bars, 20 μm. (B) Enlargement of a–d in A shows colocalization of EGFP-SV and Flag-TRIP6 with (arrowheads) and without (arrows) vinculin staining.

Discussion

We show that SV down-regulates FA structure and function, and that the mechanism involves interactions with TRIP6. Decreased levels of either protein increase cell adhesion to fibronectin. Increased SV levels decrease cell adhesion, as well as the number of stress fibers and large, mature FAs. Although more than one region of SV deleteriously affects FAs, the SV sequence with the largest effect on FA structure and function is SV342-571, which binds directly to Tctex-1 and the C-terminal LIM domains of TRIP6. SV and TRIP6 colocalize at mature FAs, and optimal SV recruitment to FAs requires binding to TRIP6. TRIP6 and the TRIP6 LIM domains partially rescue disruptive effects of SV sequences on FAs and stress fibers. Specificity is indicated by the lack of effect of Tctex-1 or the zyxin LIM domains on SV phenotypes. Thus, binding to SV342-571 is necessary, but not sufficient, to reverse SV effects on FAs.

The TRIP6 N terminus may shield the C-terminal LIM domains from SV342-571 in the absence of a regulatory signal, as has been proposed for other LIM domain proteins (Kadrmas and Beckerle, 2004; Lai et al., 2005). No direct interaction between SV sequences and the TRIP6 N terminus was detected in either yeast two-hybrid or pull-down assays. Nevertheless, full-length TRIP6 rescues the disruptive effects of longer SV proteins, implying the possibility of regulatory cross-talk between the TRIP6 N terminus and SV sequences other than SV342-571.

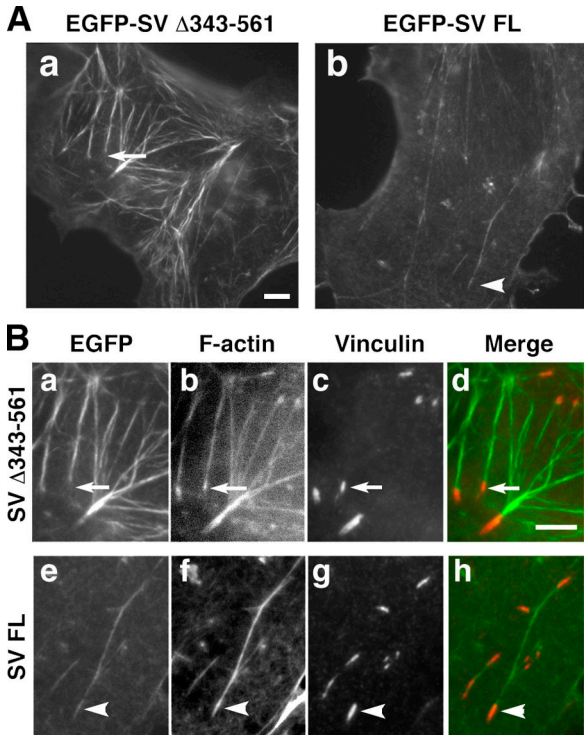

Figure 9. **SV343-561 mediates SV localization at FAs.** Reduced overlap of EGFP signal with vinculin at FAs is reduced for EGFP-SV lacking the TRIP6/Tctex-1–binding site (SVΔ343-561, arrows), as compared with full-length EGFP-SV (SV FL, arrowheads). Fluorescence micrographs of transfected COS-7 cells showing low (A) and high (B) magnification images of EGFP signals (A and B, a and e; green in d and h); phalloidin-stained F-actin (B, b and f), vinculin (B, c and g; red in d and h), and merged EGFP and vinculin channels (d and h; overlap in orange-yellow). Representative of three experiments. Bars, 5 μm.

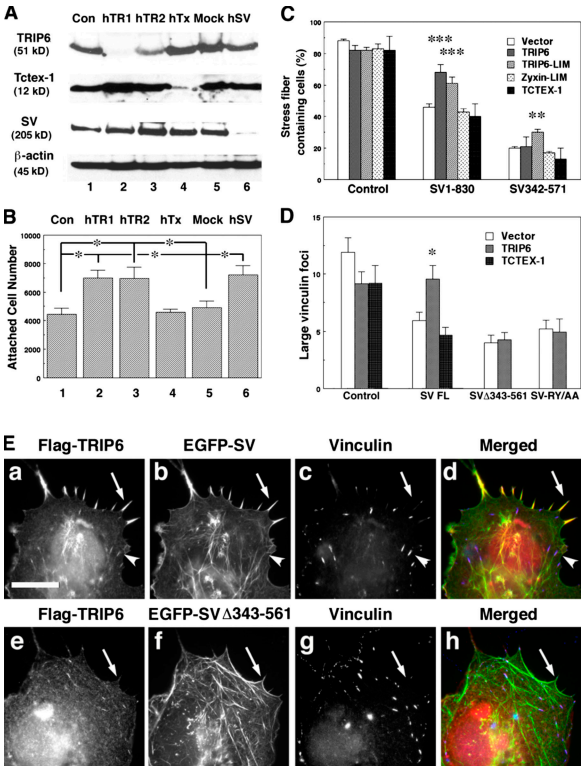

Figure 10. **TRIP6, but not Tctex-1, is involved in SV-mediated effects on adhesion.** Immunoblots of endogenous proteins in A549 cells (A) and histogram of adherent cells after centrifugation (B), showing that decreased TRIP6 or SV levels correlate with increased cell adhesion to fibronectin. Cells were treated with dsRNAs against a control sequence (A and B, lane 1; Con, hTR2 scrambled) TRIP6 (A and B, lanes 2 and 3; hTR1 and hTR2), Tctex-1 (A and B, lane 4; hTx), or SV (A and B, lane 6; hSV) or with reagent alone (A and B, lane 5; Mock). (A) Endogenous TRIP6 (51 kD), Tctex-1 (12 kD), and SV (205 kD), with β-actin (45 kD) as the loading control. (B) Adhesion assay. Mean ± the SEM. $n = 7$–8. *, $P < 0.05$. (C) Full-length TRIP6 (TRIP6) and the TRIP6 LIM domains (TRIP6-LIM) partially rescue the loss of stress fibers induced by overexpression of SV1-830; only TRIP6-LIM significantly reverses the loss of stress fibers induced by SV342-571. Zyxin LIM domains (Zyxin-LIM) and Tctex-1 (Tctex-1) have no significant effects. Neither the pcDNA3.1 vector alone (Vector) nor vectors encoding any of the candidate rescue proteins significantly affect the percentage of stress fiber–containing COS-7 cells (Control). Mean ± the SEM. $n = 3$. **, $P < 0.01$; ***, $P < 0.001$, as compared with vector only. (D) Flag-TRIP6, but not Myc-Tctex-1, partially rescues the number of large vinculin foci induced by overexpression of full-length SV (SV FL). Flag-TRIP6 has no effect on the loss of FAs induced by full-length SV mutants that lack the TRIP6-binding site (SV Δ343-561) or exhibit reduced TRIP6 binding (SV RY/AA). Mean ± the SEM. $n = 21$–25 cells per construct. *, $P < 0.05$. (E) Flag-TRIP6 (a and e; red in d and h) and full-length EGFP-SV (b; green in d) or EGFP-SVΔ343-561 (f; green in h) in COS-7 cells counterstained with anti-vinculin (c and g; blue in d and h). Bar, 20 μm. (d) Colocalization of EGFP-SV and Flag-TRIP6 with (arrowheads) and without (arrow) vinculin staining.

Observations that zyxin influences motility, adhesion, and stress fiber formation (Golsteyn et al., 1997; Hoffman et al., 2006) are reminiscent of those observed upon overexpression of SV sequences. However, SV342-571 does not bind zyxin. In conjunction with other recent observations (Petit et al., 2005), these results suggest that the members of the zyxin protein family have overlapping, but distinguishable, functions.

The loss of adhesion induced by SV overexpression apparently represents a gain of function because this phenotype is opposite that observed after SV knockdown. An SV-induced negative effect on large FAs is supported by the localization of SV with large FAs, which are structures that undergo dynamic remodeling (Ballestrem et al., 2001; Carragher and Frame, 2004). SV-mediated loss of large FAs also fits with the absence or reduced prevalence of large FAs and stress fibers in cells that contain relatively high amounts of endogenous SV, e.g., carcinomas and neutrophils (Pestonjamasp et al., 1997; Pope et al., 1998). Carcinomas and hematopoietic cells also express TRIP6 and/or LPP (Daheron et al., 2001; Xu et al., 2004), which is consistent with a physiological role for interactions with SV at dynamic FAs. Neutrophil FAs must be highly dynamic because they turn over rapidly during immune responses when little or no integrin is synthesized (Zhang et al., 2004).

Although the rescue of the SV phenotype by the TRIP6 LIM domains may be attributable to a simple dominant–negative effect on TRIP6 function (Kassel et al., 2004), the rescue by full-length TRIP6 is more interesting. In cells that overexpress both TRIP6 and wild-type SV, both proteins mislocalize into cell protrusions, sequestering SV away from FAs. Full-length SV proteins deficient in binding to TRIP6 still reduce the number of mature FAs, although these SV mutants are largely absent from FAs; TRIP6 localization at residual (or new) FAs is essentially unaffected. Thus, the FA equilibrium is disturbed by SV mutants that either contain the TRIP6-binding site out of

context or contain the other SV FA-targeting sequences in the absence of high-affinity binding to TRIP6.

The simplest interpretation of these results is that TRIP6 and SV, together with other associated proteins, act during a FA assembly/disassembly cycle to control the rate of FA turnover. In this working model, TRIP6 helps recruit SV to FAs; SV then, directly or indirectly, either blocks later stages in FA maturation and/or increases the rate of FA turnover. When SV or TRIP6 levels are limiting, cell–substrate adhesion increases because FAs are locked "on." Increasing amounts of the limiting protein decrease cell adhesion by increasing the rate of maturation of adhesive nascent FAs into less adhesive mature FAs and/or by increasing the rate of FA disassembly. In this model, TRIP6 overexpression helps restore the balance between FA assembly and disassembly in SV-overexpressing cells by (a) accelerating the formation of new FAs, (b) sequestering SV and proteins required for FA disassembly away from FAs, and/or (c) promoting the recycling of SV-associated proteins that are required for FA assembly. Overexpressed full-length SV that is deficient for binding to TRIP6 may disrupt FAs by interacting with other proteins involved in FA turnover in such a way that they become rate limiting for FA reassembly.

This model is consistent with the conflicting observations about the role of TRIP6 during cell migration. The prediction is that cellular responses to exogenous changes in TRIP6 are dependent on endogenous TRIP6 levels, relative to the levels of SV and other interactors in the proposed FA dis/assembly pathway, and on cell type–specific regulation.

We suggest that the SV–TRIP6 interaction demarcates a FA subdomain, perhaps a signaling scaffold, which controls FA integrity and/or turnover. One possibility is that the SV–TRIP6 interaction brings other SV-binding proteins into proximity with other TRIP6 partners. In addition to TRIP6, the SV N terminus (SV1-830) binds to the S2 subdomain of nonmuscle myosin II, to F-actin, and to the plasma membrane (Wulfkuhle et al., 1999; Chen et al., 2003). SV binding to TRIP6 may recruit myosin II in stress fibers into the vicinity of TRIP6-binding proteins that destabilize FAs. Candidate TRIP6 interactors include CAS/CasL (Yi et al., 2002), c-Src (Xu et al., 2004), Crk (Lai et al., 2005), the LPA_2 receptor (Xu et al., 2004), the tyrosine phosphatase PTPN13/PTP-BL/FAP-1, and the adaptor protein RIL/PDLIM4 (Cuppen et al., 2000), which is known to increase stress fiber dynamics (Vallenius et al., 2004). In agreement with this hypothesis, both SV and the LPA–TRIP6–CAS pathway positively regulate ERK signaling (Gangopadhyay et al., 2004; Lai et al., 2005), a process implicated in FA turnover (Webb et al., 2004).

Alternatively, SV binding to TRIP6 may displace a positive regulator of FA stability through steric hindrance or binding to a shared site on the TRIP6 C terminus. For instance, SV may disrupt the interaction of TRIP6 with endoglin/CD105, which is a transmembrane component of the TGF-β complex that promotes stress fiber formation and the localization of TRIP6 and zyxin to FAs (Conley et al., 2004; Sanz-Rodriguez et al., 2004).

Finally, we cannot exclude the possibility that SV indirectly influences FA structure through potentiation of TRIP6 effects in the nucleus. Despite its lack of a canonical NLS, TRIP6 can accumulate in the nucleus and modulate transcription (Kassel et al., 2004; Li et al., 2005). The TRIP6 LIM domains are sufficient for both SV binding (Fig. 6) and nuclear transport (Wang and Gilmore, 2001). SV contains functional NLS (Wulfkuhle et al., 1999) and, like TRIP6, is implicated in steroid hormone signaling (Ting et al., 2002). Thus, some of the effects reported here might be caused by changes in transcriptional activity induced by an SV–TRIP6 complex.

In summary, we show that the myosin II– and actin-binding protein SV regulates FA function through binding to TRIP6, a LIM domain–containing protein associated with signaling scaffolds that control cell motility. This is the first evidence for a myosin II–binding protein at FAs and for an explicit role for TRIP6 in adhesion. The direct binding of SV and TRIP6 suggest several specific, testable hypotheses by which TRIP6-associated scaffolds may control FA function. The SV–TRIP6 interaction may provide a "missing link" for actin-independent attachment of myosin II to the membrane at FAs and insight into molecular mechanisms for FA disassembly and/or recycling.

Materials and methods

Chemicals, proteins, and expression vectors

Chemicals were obtained from Sigma-Aldrich, Calbiochem-Novabiochem, Fisher Scientific, or VWR International, Inc., unless otherwise noted. EGFP-tagged SV constructs, purified GST-tagged SV proteins, and Flag-tagged murine TRIP6 were previously described (Wulfkuhle et al., 1999; Yi et al., 2002; Chen et al., 2003). Vectors encoding His-tagged TRIP6 LIM domains or Tctex-1 were generated by excising the insert from the pYESTrp prey vector using the vector KpnI and XhoI sites and ligating in-frame into the corresponding sites of the pET30a bacterial expression vector. The TRIP6 insert encoded amino acids 265–476, and the Tctex-1 insert was full length. Proteins tagged with 6×His were expressed and purified as previously described (Takizawa et al., 2003).

The mammalian expression vector pCMV-Myc (BD Biosciences and CLONTECH Laboratories, Inc.) was modified by inserting a HindIII restriction site into the EcoRI site in the multiple cloning sites and used to create vectors encoding N-terminal Myc-tagged proteins. Full-length Tctex-1 (aa 1–113), the TRIP6-LIM domains (aa 265–476), and zyxin-LIM domains (aa 361–562) were ligated in frame between the introduced HindIII and the endogenous XhoI restriction sites. Sequences encoding full-length Tctex-1 or the TRIP6 LIM domains were excised from isolated pYESTrp library prey vectors. The sequence encoding the zyxin LIM domains was obtained by PCR using a murine zyxin cDNA in pBluescriptII-SK(+) vector as template. All vectors were confirmed by end sequencing.

EGFP-SV lacking the TRIP6/Tctex-1–binding site (EGFP-SVΔ343-561) was created by deleting the coding sequence for aa 343–561, converting Ser 343 to a tyrosine. PCR was used to introduce an AgeI site upstream of the codon for Gly 562 in double-stranded DNA (dsDNA) that included the unique endogenous EcoRV restriction site after the codon for Asp 830 (Wulfkuhle et al., 1999). The PCR product was digested with AgeI and EcoRV and ligated into similarly cut, full-length SV in pBluescript II SK (–) (Wulfkuhle et al., 1999), replacing the codons for 343–830 with those for 562–830. SVΔ343-561 was then transferred into the mammalian expression vector EGFP-C1 (BD Biosciences and CLONTECH Laboratories, Inc.) with KpnI and XbaI.

Bovine SV sequences with reduced TRIP6/Tctex-1 binding were created by alanine replacement mutagenesis using the QuikChange Site-Directed Mutagenesis kit (Stratagene), following the manufacturer's instructions and using the following PAGE-purified primers: sense: 5′-ATGAAT GCTGCTGCTCAAACCCAGCCG-3′, and antisense: 5′-CGGCTGGGTTT-GAGCAGCAGCATT CAT-3′. Modified DNA segments were sequenced in full.

Cell culture

COS7-2 cells (Wulfkuhle et al., 1999), an SV40-transformed derivative of monkey kidney epithelial CV-1 cells, and rat A7r5 aorta cells (American

Type Culture Collection [ATCC]) were grown in DME with 10% FCS. CV-1 cells (ATCC) were maintained in MEM Alpha (Invitrogen) with 10% FCS. A549 human lung carcinoma cells (ATCC) were grown in Ham's F12K medium, 2 mM L-glutamine, and 10% FCS. Cells were transfected using Effectene Transfection Reagent (QIAGEN). Populations of 100% transfected cells were obtained by FACS 48 h after transfection with plasmids encoding EGFP or EGFP-SV.

Immunofluorescence microscopy

Methods for indirect immunofluorescence microscopy have been previously described (Chen et al., 2003). In brief, cells transfected for 24 h were fixed with 4% paraformaldehyde in PBS in the presence of 1 mM $MgCl_2$ and 1 mM EGTA for 10 min and permeabilized with 0.1% Triton X-100 in PBS for 5 (COS7-2) or 10 min (A7r5) before immunostaining. Cells were stained for vinculin (mouse clone hVIN1; 1:200; Sigma-Aldrich), Flag (rabbit polyclonal; 1:100; Sigma-Aldrich), Myc (mouse clone 9E10; 1:1,000; ATCC), Myc (rabbit monoclonal clone 71D10; Cell Signaling Technology, Inc.), TRIP6 (rabbit polyclonal B65; 1:100; Hoffman et al., 2003; or mouse anti-TRIP6, clone 16; 1:100; BD Biosciences), zyxin (rabbit polyclonal B71; 1:100; Hoffman et al., 2003), and/or SV (affinity-purified rabbit polyclonal H340; 1:100; Nebl et al., 2002; Oh et al., 2003). Cross-adsorbed secondary antibodies, conjugated with Alexa Fluor 350, 488, 568, 594, or 633 were obtained from Invitrogen. F-actin was visualized with phalloidin conjugated to Texas red or Alexa Fluor 350 (Invitrogen). Slides were analyzed at room temperature with a 100× Plan-NeoFluar oil immersion objective (NA 1.3) on a fluorescence microscope (Axioskop; both Carl Zeiss MicroImaging, Inc.) with a charge-coupled device camera (RETIGA 1300; QImaging Corp.) and OpenLab software (Improvision), or with a 100× Plan Apo oil objective, NA 1.35, on a confocal SP2 microscope (both from Leica) running Leica acquisition software. Each channel of the epifluorescence micrographs was scaled automatically using the Auto Level submenu in Photoshop 7.0 (Adobe). In Fig. 7 (c and g), the images were treated identically to show antibody specificity. Because of the high background noise in Alexa Fluor 350 images (Fig. 7, a, e, and i; Fig. 8 c, c′, g, and k; and Fig. 10 E, c and g), background noise had to be subtracted after Auto Level manipulation. This operation may also remove weak Alexa Fluor 350 signals.

Confocal single-channel optical sections were collected at excitation wavelengths of 488 nm with 12% laser power and at 633 nm with 31% laser power. Confocal images were averaged from four consecutive scans with the pinhole set to include the Airy disc 1. Within each experiment, images were collected at fixed exposures, stored in TIFF format, and manipulated identically during quantitative analyses and assembly into figures with Photoshop.

Quantification

Mean fluorescence intensities of EGFP or EGFP-SV were determined using Photoshop. Outlines of individual cells were traced manually with the lasso tool, using phase images as a reference. Mean luminosities of selected areas were determined with the histogram submenu. Estimated expression levels of EGFP-SV, relative to endogenous SV, were determined from the amounts of EGFP-SV and endogenous SV on immunoblots probed with affinity-purified H340 antibody. The ratio of EGFP-SV to endogenous SV was then compared with transfection efficiency. Typically, approximately equal amounts of EGFP-SV and endogenous SV on immunoblots were observed in cell populations with transfection efficiencies of ∼20%, for an average overexpression level of approximately sixfold in transfected cells.

The number of total and large FAs per cell were counted manually in Photoshop from images obtained at room temperature with a 25× Plan-Neofluar air objective lens (NA 0.8; Carl Zeiss MicroImaging, Inc.) on an Axioskop fluorescence microscope. FA sizes were determined by quantifying pixels in cells stained with antibody against vinculin. Because peripheral focal complexes were too numerous and/or too small to quantify, vinculin foci within 20 pixels (∼1.6 μm) of the cell border were excluded. FAs were defined as vinculin foci ≥ 30 pixels (3.75 μm^2); large FAs were those with ≥80 pixels (10 μm^2), and with pixels × mean luminosities ≥ 6,000 arbitrary units. Pixel sizes were calibrated with a micrometer.

Overlaps of EGFP signals with vinculin at FAs were assessed after the autoscaling and alignment of coded epifluorescence images in Photoshop by an author blinded to the sample identities. Images were aligned using predetermined registration shifts and checked by colocalizations of the red and green channels with blue F-actin signals. FAs were identified as vinculin foci in the red channel associated with the ends of actin filaments. Overlap of vinculin with EGFP-SVΔ343-561 or EGFP-SV in the green channel was scored on a +/− basis, with partial overlaps scored as positives.

Because of significant cytosolic distributions, colocalization of TRIP6 with vinculin at FAs was quantified as a percentage of the total lamellipodial signal. The vinculin signal between the cell periphery and the juxtanuclear region of each cell was thresholded to produce a binary mask. The percentage of the TRIP6 signal that colocalized with vinculin was calculated as a percentage of the total signal in the area under analysis divided by the percentage of total voxels under the vinculin mask. Random distributions yield ratios of ∼1.0, and colocalizations are indicated by ratios >1.0.

COS7 and human dsRNA

A ∼3.5-kb sequence encoding the 5′ end of monkey kidney SV cDNA (GenBank/EMBL/DDBJ accession no. DQ178178) was cloned by nested PCR using Herculase polymerase blend (Stratagene) and primers corresponding to SV sequences conserved in human, mouse, ferret, and bovine SV. The initial template was oligo-dT–primed, and first-strand cDNA was prepared from COS7 cell RNA using commercial kits (RNAqueous 4-PCR and Message Sensor RT-PCR; Ambion, Inc.). The first round of PCR used the primers MSV-F1 and CRATY-R (Oh et al., 2003) and a touch-down protocol, as follows: (1) 92°C, 2 min, 1×; (2) 92°C, 30 s; 55°C, 45 s; 72°C, 8 min; 5×; (3) 92°C, 30 s; 50°C, 45 s; 72°C, 8 min; 5×; (4) 92°C, 30 s; 45°C, 45 s; 72°C, 8 min; 30×; and (5) 72°C, 10 min, 1×. The reaction mixture was diluted 1:100, and 5 μl was reamplified using MSV-F1 and R-KDFW (5′-TGGCYRCCCARRAGCTTCCAGAAGTCTTT-3′) in a second touch-down reaction: (1) 95°C, 2 min, 1×; (2) 92°C, 30 s; 58°C, 45 s; 72°C, 8 min; 5×; (3) 92°C, 30 s; 55°C, 45 s; 72°C, 8 min; 5×; (4) 92°C, 30 s; 50°C, 45 s; 72°C, 8 min; 30×; and (5) 72°C, 10 min, 1×. Two clones encoding 3,524 bp of COS7 SV were sequenced and used to identify five candidate RNAi sequences (http://jura.wi.mit.edu/siRNAext; Reynolds et al., 2004).

The two most effective dsRNAs were resynthesized as Stealth duplexes (Invitrogen) and used to deplete COS7 cell SV. These dsRNAs corresponded to coding nucleotides 666–690 (dsRNA 668 sense: 5′-AGCAGCAGAGAGUUCCUCAACCUUC-3′) and 2,467–2,491 (dsRNA 2472 sense: 5′-CCCCUGGAAGAUAUCGAAGCCAGAC-3′). Control dsRNAs contained scrambled or reverse sequences, 5′-AGCGACAGAUUGUCCAACCCAGUUC-3′ (dsRNA control 668) or 5′-CCCCUGCAGACCGAAGCUAUAGAAG-3′ (dsRNA 2,472 rev, Con1). SV depletion required two dsRNA treatments over 4 d. Cells at ∼60% confluence were transfected with 10 nM dsRNA and Lipofectamine 2000 as recommended (Invitrogen), split 1:3 after 2 d, retransfected 8–10 h after splitting, and used in experiments after another 36–40 h of growth.

The same procedure was used to target human TRIP6, Tctex-1, and SV in A549 cells. hTR1(5′-AGGUCAGGAGGAGACUGUGAGAAUU-3′, coding nt 1,230–1,254) and hTR2 (5′-CGAAGAAGCUGGUUCACGACAUGAA-3′, coding nt 779–803) targeted TRIP6; hTx (5′-CAAAGUGAACCAGUGGACCACAAAU-3′, coding nt 23–47) targeted Tctex-1; and hSV (5′-GCGAUGUUUGCUGCUGGAGAGAUCA-3′, coding nt 2,026–2,050) targeted SV. Control dsRNA (Con) contained the scrambled hTR2 sequence 5′-CGACGAAUGGUCACUACAGUGAGAA-3′.

Cell adhesion and contractility

Cell–substrate adhesion was assayed by a modification of the method of Lotz et al. (1989). In brief, FACS-sorted cells expressing increased levels of EGFP-SV or EGFP, or dsRNA-treated cells (1.0×10^4 cells/ml, 3.7 ml serum-free media), were transferred into the center four wells of 24-well plates. Each well was covered with an 18-mm round coverslip (18 Circle, #1.5; VWR Scientific) coated with 10 μg/ml fibronectin. The plate was inverted and incubated for 60 min at 37°C to permit cell spreading. The plate was inverted again and centrifuged at 300 *g* for 5 min to remove unbound cells. Cells remaining on the coverslips were fixed with 4% paraformaldehyde and counted.

Cell contractility was assayed using substrate deformation assays. Flexible substrates were prepared by coating 22 × 22-mm coverslips with 0.1% gelatin (Type A; Sigma-Aldrich) on top of 5 μl silicon (30,000 CS; Dow Corning; William F. Nye Inc.). Sparsely seeded CV1 cells (<100 cells/coverslip) were allowed to attach for 30 min, transfected with plasmids encoding EGFP or EGFP-SV fragments, and grown for an additional 20 h before counting the number of fluorescent cells that were or were not associated with wrinkles, indicating the production of contractile forces (Hinz et al., 2001). The living cells were imaged at 37°C in a temperature-controlled Plexiglass chamber on an inverted microscope (DMIRE2; Leica) with a 20× air objective lens (20 DL, NA 0.4; Nikon) and a cooled charge-coupled device camera (RETIGA EXi; QImaging Corp.). Other methods were as described in the Immunofluorescence Microscopy section.

Yeast two-hybrid screens

A bait plasmid encoding bovine SV residues 171–830 was constructed in pHybLex/Zeo, transformed into the EGY48/pSH18-34 strain of *S. cerevisiae*, and used to screen a HeLa cell library in the prey vector pYESTrp (Hybrid Hunter Premade cDNA Library and Two-Hybrid System; Invitrogen) as previously described (Chen et al., 2003). In brief, a library of $\sim 1.03 \times 10^7$ primary transformants was screened approximately four times on selection medium (-ura, -trp, +Z200). Large colonies grown on induction medium (-ura, -trp, -leu, Raff/GAL,+Z200) were picked after 24 or 48 h and tested for β-galactosidase activity on modified induction medium (-ura, -trp, Raff/GAL,+Z200). Out of 506 initial colonies, 172 passed both the leucine autotrophy and β-galactosidase expression tests. Interacting prey vectors were segregated by growth for three generations on –Trp medium, recovered, electroporated into XL1 Blue cells (Stratagene), and sequenced using the pYESTrp forward primer. Sequences with an open reading frame were verified by retransformation into yeast containing the pHybLex/BSV171-830 bait vector. Nonspecific interactions were eliminated by control transformations into yeast with pHybLex/Zeo (empty bait). To localize potential binding sites, confirmed clones were transformed into yeast strains containing either pHybLexA+BSV171-342 or pHybLexA+BSV570-830, and assayed for leucine autotrophy and β-galactosidase activity.

Pull-down assays

Yeast cells (300 μl packed cell vol) expressing V5-tagged bait proteins after a 6-h induction were washed with ice-cold SLB (25 mM Tris-Cl, pH 7.5, 1 mM DTT, 2 mM EDTA, 150 mM NaCl, 30% glycerol), and protease inhibitors (1 μM aprotinin, 2 μM ALL-M, 1 mM benzamidine, 10 μM E64, 1 μM leupeptin, 1 μM pepstatin A, 1 mM PMSF). Yeast were lysed with 400 μl 0.2% Triton X-100 and SLB by vortexing three times at maximum speed for 30 s with 0.5 mm glass beads (Biospec Products Inc., Bartlesville, OK). For GST pull-down assays, COS7-2 cells (10^6 cells) were lysed with 1 ml lysis buffer (1% NP-40, 25 mM TrisCl, pH 7.5, 50 mM NaCl, 25 mM NaF, 1 mM sodium pervanadate, 50 mM sodium pyrophosphate, and the same protease inhibitors).

Lysates were centrifuged at 8,000 *g* for 7 min, and the resulting supernatants were incubated for 3 h at 0–4°C with 25 μl glutathione–Sepharose (GE Healthcare). The beads were washed once with lysis buffer and three times with washing buffer (50 mM sodium phosphate, pH 7.5, 300 mM NaCl, and 10% glycerol and 2-mercaptoethanol). Bound proteins were eluted with 20 mM glutathione in washing buffer, resolved by SDS-PAGE, and transferred to nitrocellulose membranes (Protran BA85; Schleicher & Schuell BioScience, Inc.).

Immunoblots

Glutathione-eluted proteins blotted to nitrocellulose were stained for Flag-tag (rabbit polyclonal; 1:1,000; Sigma), Myc-tag (mouse clone 9E10; 1:10,000; ATCC), V5-tag (mouse monoclonal; 1:200; Invitrogen), 6×His-tag (mouse clone 27E8; 1:1,000; Cell Signaling Technology), GST (goat polyclonal; 1:1,000; GE Healthcare) or GFP (mouse clones 7.1 and 13.1; 1:3,000; Roche). Immuno–cross-adsorbed secondary antibodies conjugated to HRP were obtained from Jackson ImmunoResearch. Signals were detected by ECL (Pierce Chemical Co.).

Endogenous proteins in mammalian cell lysates were analyzed after extraction and precipitation with 10% TCA (Takizawa et al., 2003). Blot strips were stained with antibodies against SV (rabbit polyclonal H340; 1:10,000), β-actin (mouse clone AC-74; 1:3,000; Sigma- Aldrich), zyxin (rabbit polyclonal B71; 1:5,000), TRIP6/ZRP-1 (rabbit polyclonal B65; 1:2,000; and mouse monoclonal C.16; 1:2,000), or Tctex-1 (rabbit polyclonal R5205;, 1:25; King et al., 1996). R5205 was provided by S.M. King (University of Connecticut Health Center, Farmington, CT).

Binding and competition assays

Purified (100 μg) 6×His-tagged TRIP6 LIM domains or 6×His-tagged, full-length Tctex-1 protein were incubated with ~0.6 nmol GST-SV343-571 (30 μg) or GST (15 μg) on glutathione–Sepharose (25 μl). Bound proteins were sedimented, washed, eluted, and analyzed by SDS-PAGE and staining with Coomassie brilliant blue or anti-6×His antibody. In competition assays, 6×His-TRIP6 LIM domains (100 μg; 5 nmol) were incubated with GST-SV343-571 (30 μg; 0.6 nmol) on glutathione–Sepharose (25 μl) in the presence of increasing amounts of premixed 6×His-Tctex-1: 0, 10 (0.8 nmol), 20 (1.5 nmol), and 100 μg (7.7 nmol).

Online supplemental material

Fig. S1 shows EGFP-SV overlap with vinculin-stained FAs at the basal surface of a COS-7 cell. Fig. S2 shows that the RY/AA mutant of EGFP-SV342-571 exhibits a less deleterious phenotype than EGFP-SV342-571 on stress fibers and large FAs. Fig. S3 shows the specificities of the antibodies used in this study on COS7 and A7r5 cells. Fig. S4 shows that TRIP6 remains at FAs after SV knockdown. Online supplemental material is available at http://www.jcb.org/cgi/content/full/jcb.200512051.

We gratefully acknowledge Dr. Peter Pryciak for advice and assistance with the yeast two-hybrid assays, Dr. Roger Davis for access to the confocal microscope, Dr. Stephen King for the gift of the Tctex-1 antibody, and the UMMS FACS core facility. We also thank Louise Ohrn for solution preparation and Donna Castellanos for expert glassware preparation.

This publication was supported by National Institutes of Health (NIH) grants GM33048 (E.J. Luna) and GM50877 (M.C. Beckerle) and benefited from NIH grant DK060564 to the University of Massachusetts Medical School Biomedical Imaging Group (L.M. Lifshitz).

The contents of this work are solely the responsibility of the authors and do not necessarily represent the official views of the NIH.

Submitted: 9 December 2005
Accepted: 25 June 2006

References

Alahari, S.K., P.J. Reddig, and R.L. Juliano. 2002. Biological aspects of signal transduction by cell adhesion receptors. *Int. Rev. Cytol.* 220:145–184.

Ballestrem, C., B. Hinz, B.A. Imhof, and B. Wehrle-Haller. 2001. Marching at the front and dragging behind: differential αVβ3-integrin turnover regulates focal adhesion behavior. *J. Cell Biol.* 155:1319–1332.

Beningo, K.A., M. Dembo, I. Kaverina, J.V. Small, and Y.L. Wang. 2001. Nascent focal adhesions are responsible for the generation of strong propulsive forces in migrating fibroblasts. *J. Cell Biol.* 153:881–888.

Carragher, N.O., and M.C. Frame. 2004. Focal adhesion and actin dynamics: a place where kinases and proteases meet to promote invasion. *Trends Cell Biol.* 14:241–249.

Chen, Y., N. Takizawa, J.L. Crowley, S.W. Oh, C.L. Gatto, T. Kambara, O. Sato, X. Li, M. Ikebe, and E.J. Luna. 2003. F-actin and myosin II binding domains in supervillin. *J. Biol. Chem.* 278:46094–46106.

Conley, B.A., R. Koleva, J.D. Smith, D. Kacer, D. Zhang, C. Bernabeu, and C.P. Vary. 2004. Endoglin controls cell migration and composition of focal adhesions: function of the cytosolic domain. *J. Biol. Chem.* 279:27440–27449.

Cuppen, E., M. van Ham, D.G. Wansink, A. de Leeuw, B. Wieringa, and W. Hendriks. 2000. The zyxin-related protein TRIP6 interacts with PDZ motifs in the adaptor protein RIL and the protein tyrosine phosphatase PTP-BL. *Eur. J. Cell Biol.* 79:283–293.

Daheron, L., A. Veinstein, F. Brizard, H. Drabkin, L. Lacotte, F. Guilhot, C.J. Larsen, A. Brizard, and J. Roche. 2001. Human LPP gene is fused to MLL in a secondary acute leukemia with a t(3;11) (q28;q23). *Genes Chromosomes Cancer*. 31:382–389.

Galbraith, C.G., K.M. Yamada, and M.P. Sheetz. 2002. The relationship between force and focal complex development. *J. Cell Biol.* 159:695–705.

Gangopadhyay, S.S., N. Takizawa, C. Gallant, A.L. Barber, H.D. Je, T.C. Smith, E.J. Luna, and K.G. Morgan. 2004. Smooth muscle archvillin: A novel regulator of signaling and contractility in vascular smooth muscle. *J. Cell Sci.* 117:5043–5057.

Golsteyn, R.M., M.C. Beckerle, T. Koay, and E. Friederich. 1997. Structural and functional similarities between the human cytoskeletal protein zyxin and the ActA protein of *Listeria monocytogenes*. *J. Cell Sci.* 110:1893–1906.

Guryanova, O.A., A.A. Sablina, P.M. Chumakov, and E.I. Frolova. 2005. Down-regulation of *TRIP6* gene expression induces actin cytoskeleton rearrangements in human carcinoma cell lines. *Mol. Biol.* 39:792–795.

Harris, B.Z., and W.A. Lim. 2001. Mechanism and role of PDZ domains in signaling complex assembly. *J. Cell Sci.* 114:3219–3231.

Hinz, B., G. Celetta, J.J. Tomasek, G. Gabbiani, and C. Chaponnier. 2001. Alpha-smooth muscle actin expression upregulates fibroblast contractile activity. *Mol. Biol. Cell*. 12:2730–2741.

Hoffman, L.M., C.C. Jensen, S. Kloeker, C.L. Wang, M. Yoshigi, and M.C. Beckerle. 2006. Genetic ablation of zyxin causes Mena/VASP mislocalization, increased motility, and deficits in actin remodeling. *J. Cell Biol.* 172:771–782.

Hoffman, L.M., D.A. Nix, B. Benson, R. Boot-Hanford, E. Gustafsson, C. Jamora, A.S. Menzies, K.L. Goh, C.C. Jensen, F.B. Gertler, et al. 2003. Targeted disruption of the murine zyxin gene. *Mol. Cell. Biol.* 23:70–79.

Hogg, N., A. Smith, A. McDowall, K. Giles, P. Stanley, M. Laschinger, and R. Henderson. 2004. How T cells use LFA-1 to attach and migrate. *Immunol. Lett.* 92:51–54.

Kadrmas, J.L., and M.C. Beckerle. 2004. The LIM domain: from the cytoskeleton to the nucleus. *Nat. Rev. Mol. Cell Biol.* 5:920–931.

Kassel, O., S. Schneider, C. Heilbock, M. Litfin, M. Gottlicher, and P. Herrlich. 2004. A nuclear isoform of the focal adhesion LIM-domain protein Trip6 integrates activating and repressing signals at AP-1- and NF-kappaB-regulated promoters. *Genes Dev.* 18:2518–2528.

Kaverina, I., O. Krylyshkina, and J.V. Small. 2002. Regulation of substrate adhesion dynamics during cell motility. *Int. J. Biochem. Cell Biol.* 34:746–761.

King, S.M., J.F. Dillman III, S.E. Benashski, R.J. Lye, R.S. Patel-King, and K.K. Pfister. 1996. The mouse t-complex-encoded protein Tctex-1 is a light chain of brain cytoplasmic dynein. *J. Biol. Chem.* 271:32281–32287.

Lai, Y.J., C.S. Chen, W.C. Lin, and F.T. Lin. 2005. c-Src-mediated phosphorylation of TRIP6 regulates its function in lysophosphatidic acid-induced cell migration. *Mol. Cell. Biol.* 25:5859–5868.

Lele, T.P., J. Pendse, S. Kumar, M. Salanga, J. Karavitis, and D.E. Ingber. 2006. Mechanical forces alter zyxin unbinding kinetics within focal adhesions of living cells. *J. Cell. Physiol.* 207:187–194.

Li, L., L.H. Bin, F. Li, Y. Liu, D. Chen, Z. Zhai, and H.B. Shu. 2005. TRIP6 is a RIP2-associated common signaling component of multiple NF-kappaB activation pathways. *J. Cell Sci.* 118:555–563.

Lotz, M.M., C.A. Burdsal, H.P. Erickson, and D.R. McClay. 1989. Cell adhesion to fibronectin and tenascin: quantitative measurements of initial binding and subsequent strengthening response. *J. Cell Biol.* 109:1795– 1805.

Murthy, K.K., K. Clark, Y. Fortin, S.H. Shen, and D. Banville. 1999. ZRP-1, a zyxin-related protein, interacts with the second PDZ domain of the cytosolic protein tyrosine phosphatase hPTP1E. *J. Biol. Chem.* 274:20679– 20687.

Nebl, T., K.N. Pestonjamasp, J.D. Leszyk, J.L. Crowley, S.W. Oh, and E.J. Luna. 2002. Proteomic analysis of a detergent-resistant membrane skeleton from neutrophil plasma membranes. *J. Biol. Chem.* 277:43399–43409.

Oh, S.W., R.K. Pope, K.P. Smith, J.L. Crowley, T. Nebl, J.B. Lawrence, and E.J. Luna. 2003. Archvillin, a muscle-specific isoform of supervillin, is an early expressed component of the costameric membrane skeleton. *J. Cell Sci.* 116:2261–2275.

Pestonjamasp, K.N., R.K. Pope, J.D. Wulfkuhle, and E.J. Luna. 1997. Supervillin (p205): A novel membrane-associated, F-actin–binding protein in the villin/gelsolin superfamily. *J. Cell Biol.* 139:1255–1269.

Petit, M.M., S.M. Meulemans, and W.J. Van de Ven. 2003. The focal adhesion and nuclear targeting capacity of the LIM-containing lipoma-preferred partner (LPP) protein. *J. Biol. Chem.* 278:2157–2168.

Petit, M.M., K.R. Crombez, H.B. Vervenne, N. Weyns, and W.J. Van de Ven. 2005. The tumor suppressor Scrib selectively interacts with specific members of the zyxin family of proteins. *FEBS Lett.* 579:5061–5068.

Pope, R.K., K.N. Pestonjamasp, K.P. Smith, J.D. Wulfkuhle, C.P. Strassel, J.B. Lawrence, and E.J. Luna. 1998. Cloning, characterization, and chromosomal localization of human supervillin (SVIL). *Genomics*. 52:342–351.

Reynolds, A., D. Leake, Q. Boese, S. Scaringe, W.S. Marshall, and A. Khvorova. 2004. Rational siRNA design for RNA interference. *Nat. Biotechnol.* 22:326–330.

Ridley, A.J., M.A. Schwartz, K. Burridge, R.A. Firtel, M.H. Ginsberg, G. Borisy, J.T. Parsons, and A.R. Horwitz. 2003. Cell migration: integrating signals from front to back. *Science*. 302:1704–1709.

Sanz-Rodriguez, F., M. Guerrero-Esteo, L.M. Botella, D. Banville, C.P. Vary, and C. Bernabeu. 2004. Endoglin regulates cytoskeletal organization through binding to ZRP-1, a member of the Lim family of proteins. *J. Biol. Chem.* 279:32858–32868.

Takizawa, N., D.J. Schmidt, K. Mabuchi, E. Villa-Moruzzi, R.A. Tuft, and M. Ikebe. 2003. M20, the small subunit of PP1M, binds to microtubules. *Am. J. Physiol. Cell Physiol.* 284:C250–C262.

Ting, H.J., S. Yeh, K. Nishimura, and C. Chang. 2002. Supervillin associates with androgen receptor and modulates its transcriptional activity. *Proc. Natl. Acad. Sci. USA*. 99:661–666.

Vallenius, T., B. Scharm, A. Vesikansa, K. Luukko, R. Schafer, and T.P. Makela. 2004. The PDZ-LIM protein RIL modulates actin stress fiber turnover and enhances the association of alpha-actinin with F-actin. *Exp. Cell Res.* 293:117–128.

Wang, Y., and T.D. Gilmore. 2001. LIM domain protein Trip6 has a conserved nuclear export signal, nuclear targeting sequences, and multiple transactivation domains. *Biochim. Biophys. Acta*. 1538:260–272.

Wang, Y., and T.D. Gilmore. 2003. Zyxin and paxillin proteins: focal adhesion plaque LIM domain proteins go nuclear. *Biochim. Biophys. Acta*. 1593:115–120.

Webb, D.J., K. Donais, L.A. Whitmore, S.M. Thomas, C.E. Turner, J.T. Parsons, and A.F. Horwitz. 2004. FAK-Src signalling through paxillin, ERK and MLCK regulates adhesion disassembly. *Nat. Cell Biol.* 6:154–161.

Williams, J.M., G.C. Chen, L. Zhu, and R.F. Rest. 1998. Using the yeast two-hybrid system to identify human epithelial cell proteins that bind gonococcal Opa proteins: intracellular gonococci bind pyruvate kinase via their Opa proteins and require host pyruvate for growth. *Mol. Microbiol.* 27:171–186.

Wulfkuhle, J.D., I.E. Donina, N.H. Stark, R.K. Pope, K.N. Pestonjamasp, M.L. Niswonger, and E.J. Luna. 1999. Domain analysis of supervillin, an F-actin bundling plasma membrane protein with functional nuclear localization signals. *J. Cell Sci.* 112:2125–2136.

Xu, J., Y.J. Lai, W.C. Lin, and F.T. Lin. 2004. TRIP6 enhances lysophosphatidic acid-induced cell migration by interacting with the lysophosphatidic acid 2 receptor. *J. Biol. Chem.* 279:10459–10468.

Yi, J., and M.C. Beckerle. 1998. The human TRIP6 gene encodes a LIM domain protein and maps to chromosome 7q22, a region associated with tumorigenesis. *Genomics*. 49:314–316.

Yi, J., S. Kloeker, C.C. Jensen, S. Bockholt, H. Honda, H. Hirai, and M.C. Beckerle. 2002. Members of the Zyxin family of LIM proteins interact with members of the p130Cas family of signal transducers. *J. Biol. Chem.* 277:9580–9589.

Yoshigi, M., L.M. Hoffman, C.C. Jensen, H.J. Yost, and M.C. Beckerle. 2005. Mechanical force mobilizes zyxin from focal adhesions to actin filaments and regulates cytoskeletal reinforcement. *J. Cell Biol.* 171:209–215.

Zaidel-Bar, R., M. Cohen, L. Addadi, and B. Geiger. 2004. Hierarchical assembly of cell-matrix adhesion complexes. *Biochem. Soc. Trans.* 32:416–420.

Zhang, X., Y. Kluger, Y. Nakayama, R. Poddar, C. Whitney, A. DeTora, S.M. Weissman, and P.E. Newburger. 2004. Gene expression in mature neutrophils: early responses to inflammatory stimuli. *J. Leukoc. Biol.* 75:358–372.

Zumbrunn, J., and B. Trueb. 1996. A zyxin-related protein whose synthesis is reduced in virally transformed fibroblasts. *Eur. J. Biochem.* 241:657–663.